

A combined magnetic field stabilization system for improving the stability of $^{40}Ca^{+}$ optical clock

Mengyan Zeng(曾孟彦), Zixiao Ma(马子晓), Ruming Hu(胡如明), Baolin Zhang(张宝林), Yanmei Hao(郝艳梅), Huaqing Zhang(张华青), Yao Huang(黄垚), Hua Guan(管桦), and Kelin Gao(高克林)
Citation: Chin. Phys. B, 2023, 32 (**11**): 110704. DOI: 10.1088/1674-1056/acf5d5
Journal homepage: http://cpb.iphy.ac.cn; http://iopscience.iop.org/cpb

What follows is a list of articles you may be interested in

Residual field suppression for magnetocardiography measurement inside a thin magnetically shielded room using bi-planar coil

Kang Yang(杨康), Hong-Wei Zhang(张宏伟), Qian-Nian Zhang(张千年),Jun-Jun Zha(查君君), and Deng-Chao Huang(黄登朝)
Chin. Phys. B, 2022, 31 (**7**): 070701. DOI: 10.1088/1674-1056/ac6163

Performance study of aluminum shielded room for ultra-low-field magnetic resonance imaging based on SQUID: Simulations and experiments

Bo Li(李波), Hui Dong(董慧), Xiao-Lei Huang(黄小磊), Yang Qiu(邱阳), Quan Tao(陶泉), Jian-Ming Zhu(朱建明)
Chin. Phys. B, 2018, 27 (**2**): 020701. DOI: 10.1088/1674-1056/27/2/020701

Relationship measurement between ac-Stark shift of $^{40}Ca^{+}$ clock transition and laser polarization direction

Hong-Fang Song(宋红芳), Shao-Long Chen(陈邵龙), Meng-Yan Zeng(曾孟彦), Yao Huang(黄垚), Hu Shao(邵虎), Yong-Bo Tang(唐永波), Hua Guan(管桦), Ke-Lin Gao(高克林)
Chin. Phys. B, 2017, 26 (**9**): 099501. DOI: 10.1088/1674-1056/26/9/099501

Correlation between the magic wavelengths and the polarization direction of the linearly polarized laser in the Ca^{+} optical clock

Liu Pei-Liang (刘培亮), Huang Yao (黄垚), Bian Wu (边武), Shao Hu (邵虎), Qian Yuan (钱源), Guan Hua (管桦), Tang Li-Yan (唐丽艳), Gao Ke-Lin (高克林)
Chin. Phys. B, 2015, 24 (**3**): 039501. DOI: 10.1088/1674-1056/24/3/039501

Dependence of the ^{85}Rb coherent population trapping resonance characteristic on the pressure of N_2 buffer gas

Qu Su-Ping (屈苏平), Zhang Yi (张奕), Gu Si-Hong (顾思洪)
Chin. Phys. B, 2013, 22 (**9**): 099501. DOI: 10.1088/1674-1056/22/9/099501

INSTRUMENTATION AND MEASUREMENT

A combined magnetic field stabilization system for improving the stability of $^{40}Ca^{+}$ optical clock

Mengyan Zeng(曾孟彦)[1,2,3,†], Zixiao Ma(马子晓)[2,3,4,†], Ruming Hu(胡如明)[2,3,4], Baolin Zhang(张宝林)[2,3], Yanmei Hao(郝艳梅)[2,3,4], Huaqing Zhang(张华青)[2,3], Yao Huang(黄垚)[2,3], Hua Guan(管桦)[2,3,5,‡], and Kelin Gao(高克林)[2,3,§]

[1] *Huazhong University of Science and Technology, Wuhan* 430074, *China*
[2] *State Key Laboratory of Magnetic Resonance and Atomic and Molecular Physics, Innovation Academy for Precision Measurement Science and Technology, Chinese Academy of Sciences, Wuhan* 430071, *China*
[3] *Key Laboratory of Atomic Frequency Standards, Innovation Academy for Precision Measurement Science and Technology, Chinese Academy of Sciences, Wuhan* 430071, *China*
[4] *University of Chinese Academy of Sciences, Beijing* 100049, *China*
[5] *Wuhan Institute of Quantum Technology, Wuhan* 430206, *China*

(Received 13 July 2023; revised manuscript received 23 August 2023; accepted manuscript online 1 September 2023)

Future applications of portable $^{40}Ca^{+}$ optical clocks require reliable magnetic field stabilization to improve frequency stability, which can be achieved by implementing an active and passive magnetic field noise suppression system. On the one hand, we have optimized the magnetic shielding performance of the portable optical clock by reducing its apertures and optimizing its geometry; on the other hand, we have introduced an active magnetic field noise suppression system to further suppress the magnetic field noise experienced by the ions. These efforts reduced the ambient magnetic field noise by about 10000 times, significantly reduced the linewidth of the clock transition spectrum, improved the stability of the portable $^{40}Ca^{+}$ optical clock, and created the conditions for using portable optical clocks in non-laboratory magnetic field environments. This active magnetic field suppression scheme has the advantages of simple installation and wide applicability.

Keywords: $^{40}Ca^{+}$ optical clock, magnetic field compensation, frequency stability

PACS: 07.55.Nk, 95.55.Sh **DOI:** 10.1088/1674-1056/acf5d5

1. Introduction

Optical atomic clocks have developed rapidly in the past two decades with the advancement of laser technology. To date, single-ion clocks based on Al^{+},[1,2] Yb^{+},[3] Ca^{+},[4,5] Lu^{+}[6] and optical lattice clocks based on Yb,[7] Sr[8–10] have demonstrated fractional uncertainties of 10^{-18} level or below. Such optical clocks have outperformed the cesium fountain primary standard by two orders of magnitude, facilitating the discussion of redefining the second with optical clocks.[11] High-precision optical clocks have also become an indispensable technology for the precise measurement of physical quantities and have advanced our understanding of physics.[12–14] In addition to the ever-increasing precision of optical clocks, applications of portable optical clocks are also a future development trend of optical clocks. At present, although optical clock comparisons based on free space links and fiber links have achieved relatively high accuracy,[15,16] these techniques are limited by geographical or climatic factors over long distances. The development of optical clocks that can be transported over long distances is still of great importance to the fields of precision measurement and time keeping. Among them, $^{40}Ca^{+}$ is an ideal candidate for portable optical clocks due to the advantages of simple laser structure and low laser power. So far, the Sr and Ca^{+} optical clocks based on the vehicle platform have achieved some significant results after long-distance transportation.[17,18] On the other hand, the Sr and Ca^{+} optical clocks for portable applications have achieved uncertainties of 10^{-18} level.[5,9]

In contrast to other optical atomic clocks being investigated, the reference transition of the $^{40}Ca^{+}$ optical clock has a linear Zeeman sensitivity to the ambient magnetic field.[19] Its clock transition can be split into 10 Zeeman components under weak magnetic field conditions. To cancel the first-order Zeeman shift, the electric quadrupole shift, and the tensor Stark shifts, three pairs of Zeeman components are required to be investigated simultaneously.[19] All the Zeeman components of the clock transition are sensitive to the magnetic field, since the $^{40}Ca^{+}$ has the nuclear spin of zero. Although the uncertainty of the portable $^{40}Ca^{+}$ optical clocks has been evaluated to 4.8×10^{-18}, it is difficult to achieve a comparable statis-

†Mengyan Zeng and Zixiao Ma contributed equally to this work.
‡Corresponding author. E-mail: guanhua@apm.ac.cn
§Corresponding author. E-mail: klgao@apm.ac.cn

© 2023 Chinese Physical Society and IOP Publishing Ltd

tical accuracy with this uncertainty level due to the poor stability, which is mainly limited by the magnetic field noise.[5] Specifically, the magnetic field noise broadens the spectral lines of the clock transition, making it difficult to obtain a narrow linewidth transition. Moreover, it can also cause fringe slipping when the Ramey interrogation has been applied and reduces the continuous operation rate.[20] The Allan deviation results obtained by comparing a portable $^{40}Ca^{+}$ optical clock in a non-laboratory environment with a laboratory clock are not as good as those obtained by comparing two optical clocks in a laboratory environment.[20]

In laboratory environments, the dominant magnetic noise comes mainly from the geomagnetic fields, other nearby instruments, and magnetized objects, and is generally suppressed by magnetic shields.[4,21] However, for portable optical clocks in non-laboratory environments,[18,22] and even for future space-based optical clocks,[23] the sources of magnetic field noise will be more complex and variable.[24] To this end, improved magnetic shields and an active magnetic field compensation system are employed, which is expected to keep the magnetic field experienced by the ions sufficiently static and stable in different application environments.

Through these efforts, we have attenuated the magnetic field noise by more than 300 times through improved passive magnetic shields, and then used an active magnetic field noise suppression device to suppress the attenuated magnetic field noise by about 30 times, that is, the total magnetic field noise of the external environment has been reduced by about 10000 times. Experiments show that when the external magnetic field source is far away from the optical clock, the magnetic field stabilization system proposed in this paper effectively suppresses the external magnetic field noise and achieves a measurement result of stability of $2.5\times10^{-15}/\sqrt{\tau}$.

2. Passive magnetic shielding system

High performance magnetic shields are the starting point for effective suppression of magnetic field noise. In addition, applications for portable optical clocks require them to be rugged, compact, and small in size while providing ample optical access. Details of the design, construction, and performance of the improved magnetic shields for the portable optical clock are shown below. The performance of the magnetic shields depends on three main aspects: the shape of the shield, the physical parameters of the material, and the geometric constraints of the experiment.[25] The former determines the trade-off between shielding efficiency and saturation tolerance. The latter is determined by the need for optical and electrical access and the geometry of the vacuum chamber. For the second, the permalloy material used in the magnetic shields of the $^{40}Ca^{+}$ optical clock is vacuum melted and then high temperature annealed in pure hydrogen. It has an initial relative permeability μ_r greater than 10^5, allowing it to redirect the magnetic flux lines around the enclosed volume. The ideal shape for a magnetic shield is a sphere or an infinitely long cylinder, since sharp corners often cause flux leakage. At the same time, its overall size should be as small as possible, since the attenuation of the external magnetic field $A=\mu_r d/(2R)$ is inversely proportional to the shield radius R for a given thickness d.[26] Therefore, the magnetic shields of the $^{40}Ca^{+}$ optical clock adopt an approximate long cylinder design, and the radius of the cylinder R is reduced as much as possible to 88 mm. The overall size of the outermost layer of the magnetic shields is only $\pi\times(88\ \text{mm})^2\times375$ mm.

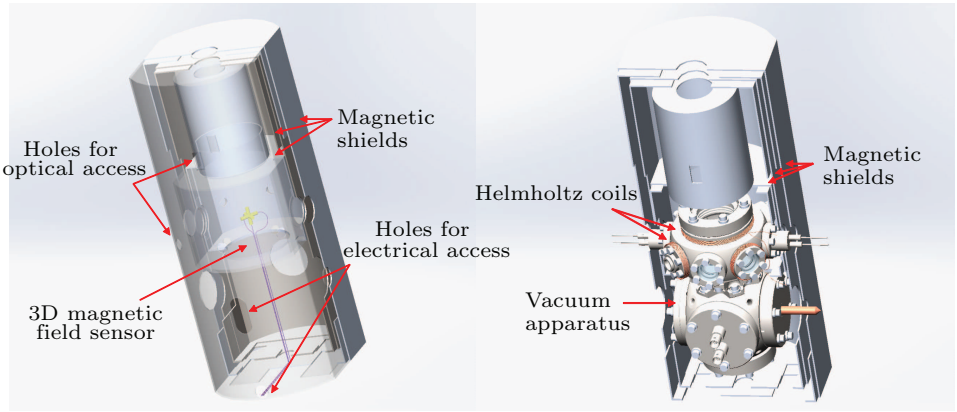


Fig. 1. Schematic diagram of the overall configuration within the three-layer magnetic shield. The vacuum chamber and associated fixtures are made of non-magnetic titanium, which provides low outgassing and reduces system weight compared to non-magnetic stainless steel designs. The vacuum ion trap system is used for the long-term stable trapping of calcium ions, the details of which can be found in our previous work.[4,5] Three pairs of Helmholtz coils are installed inside the shields on the titanium vacuum chamber to adjust the magnitude and direction of the magnetic field felt by the $^{40}Ca^{+}$ ion.

The main limitation of the shield geometry is the dimensions of the ultra-high-vacuum (UHV) chamber containing the ion trap system. It cannot be completely hermetic because the experiments require optical access to the $^{40}Ca^{+}$ ion for laser manipulation and electrical access to the ion trap. The magnetic shield design has six 10 mm diameter holes for the op-

tical access at the position corresponding to the height of the optical window of the vacuum chamber, and two 30 mm diameter holes for the RF electrodes and the compensation electrodes of the ion trap. In addition, there is another 30 mm diameter hole directly above for ion fluorescence signal acquisition, and some openings on the bottom side away from the ion trap for external extensions of the vacuum system. The necessary access limits the effect of further increasing the number of magnetic shielding layers to passively reduce the external magnetic field. What's more, since the magnetic shields need to be easily disassembled for transport of the optical clock, we chose the magnetic shields design with three or four layers. Using a three-axis magnetic field sensor, we measured that the three-layer magnetic shield shown in Fig. 1 has shielding factors of 578, 354, and 321 in the axial direction and the two radial directions, respectively. Future improvements in magnetic shields can be achieved by increasing the number of layers and optimizing the spacing of each pair of adjacent layers within a limited volume.[27]

3. Active magnetic shielding system

For practical applications of portable $^{40}Ca^{+}$ optical clocks, a passive magnetic field shielding system alone is usually not sufficient to reduce the transition spectral linewidth to the Hertz level in complex external magnetic field environments. Therefore, the noise attenuated by the magnetic shields is further suppressed by an active noise compensation device, which converts the magnetic field noise signal into a current signal and applies it to the Helmholtz coils to actively compensate for the magnetic field noise. Similar to most active magnetic field stabilization methods,[28–30] the limitation of this scheme is that if the magnetometer cannot be located at the site of the ion, the magnetic field at the sensor may not perfectly track the magnetic field felt by the ion, resulting in imperfect noise suppression. Fortunately, the magnetic field noise at the ion's position can be considered to be consistent with the external magnetic field noise, since the source of the magnetic field noise is generally far away from the system.

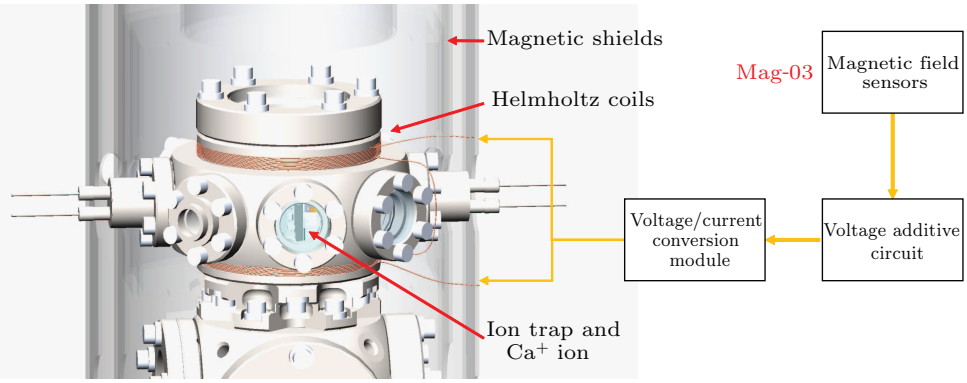


Fig. 2. Schematic diagram of the active magnetic field noise suppression system. The three-axis magnetic field sensors (Bartington Ins., Mag-03) used in the active compensation scheme consist of the fluxgate sensors and the data acquisition units to provide precision measurements of static and alternating magnetic fields in three axes. These sensors can be combined with a voltage summation circuit and a voltage/current conversion module to form a complete magnetic field noise compensation system.

The measurement results of the magnetic field at different positions show that the magnitude and trend of the magnetic field noise near the portable optical clock are almost the same. The magnetic field noise after passing through the magnetic shielding layers has different components in different directions, but the trends are measured to be the same. Then, the magnetic field of the ion position can be expressed as

$$\boldsymbol{B} = (B_x + k_x \Delta B)\hat{x} + (B_y + k_y \Delta B)\hat{y} + (B_z + k_z \Delta B)\hat{z}, \quad (1)$$

where B_i $(i = x, y, z)$ are the static magnetic field components of the x, y and z directions attenuated by the magnetic shields, ΔB indicates the magnitude of the external magnetic field noise, and k_i $(i = x, y, z)$ are the shielding coefficients of the magnetic shields against the magnetic field noise in the three directions.

Because a magnetic field sensor cannot be mounted on the ion trap, we cannot directly measure the magnetic field intensity and noise at the center of the ion trap. Therefore, conventional proportional integration circuits cannot be used to suppress the magnetic field noise felt by the ion. Experimentally, the DC components of the magnitude field B_i $(i = x, y, z)$ can be obtained from the Zeeman components of the clock transition, and the external magnetic field noise component ΔB can be measured by the fluxgate. These fluxgate sensors can be used for magnetic field measurement applications from pT up to 1 mT with the noise levels of $>$ 10 to 20 pTrms/$\sqrt{\text{Hz}}$ at 1 Hz. The measured external magnetic field signal is converted to a voltage output by the data acquisition units, and the noise signal is separated by a voltage summation circuit. The noise voltage is then applied to a pair of Helmholtz coils by connecting a wide range variable resistor (Bourns, standard resistance range of 10 Ω to 10 kΩ for 25 rounds) in series. Finally, a reverse magnetic field fluctuation is generated at the center of the ion trap by the Helmholtz coils, and an appropri-

ate magnetic field noise gain coefficient k can be obtained by adjusting the resistance value of the variable resistor. When the compensation magnetic field signal is applied in the z direction, the total magnetic field felt by the ion can be expressed as

$$\begin{aligned}\boldsymbol{B}' &= (B_x + k_x\Delta B)\hat{x} + (B_y + k_y\Delta B)\hat{y} \\ &\quad + (B_z + k_z\Delta B + k\Delta B)\hat{z}. \end{aligned} \tag{2}$$

Due to the Zeeman effect, the DC components of the magnetic field split the Zeeman components of the clock transition, and the noise component broadens the transition line shape, and their effects are approximately 0.1 MHz and 10 Hz for the former and the latter, respectively. Therefore, we have

$$B_i \gg k_i\Delta B, \quad (i = x, y, z). \tag{3}$$

The noise also has little effect on the direction of the bias magnetic field. The magnitude of the total magnetic field is close to

$$\begin{aligned}\left|\boldsymbol{B}'\right|^2 &\approx B_x^2 + B_y^2 + B_z^2 \\ &\quad + 2(k_xB_x + k_yB_y + k_zB_z + kB_z)\Delta B. \end{aligned} \tag{4}$$

When

$$k_xB_x + k_yB_y + k_zB_z + kB_z = 0, \tag{5}$$

the effect of the magnetic field noise is canceled. The parameters k_x, k_y and k_z are determined by the performance of the magnetic shields and can be considered stable. The gain coefficient k can be adjusted by adjusting the resistance value of the variable resistor and the direction of the current until Eq. (5) holds. Experimentally, the parameters of the active magnetic field noise suppression device are optimized by minimizing the corresponding linewidth of the clock transition. Therefore, the noise suppression effect can also be evaluated by the linewidth of the clock transition.

4. Stability improvement by the passive and active magnetic field suppression scheme

The shielding factors of the magnetic shields have been measured by placing flux gates inside and outside the magnetic shield (as shown in the left panel of Fig. 1). However, the performance of the active magnetic field suppression system is related to the magnetic fields of the ion position, the Helmholtz coils of the optical clock and its position with the ion position, and is difficult to measure directly. Therefore, we evaluate the performance of the active magnetic field suppression system by measuring the multiple of the linewidth that is narrowed. Due to the appearance of a new magnetic field source (the source may be the subway running) at a large distance from the outside, the interference of the new magnetic field noise source reduces the optical clock interrogation time of the current experiment compared to the previous 80 ms optical clock interrogation time under good laboratory conditions.[4,20] Figure 3 shows the measurement results of the magnetic field around the optical clock system in 2 days. For the $^2S_{1/2}(m_J = \pm 1/2)$– $^2D_{5/2}(m_J = \pm 5/2)$ transition in the three pairs of Zeeman components most affected by magnetic field noise, the maximum interrogation time is limited to 5 ms when the magnetic field environment deteriorates. Therefore, we further suppress the external noise through active compensation based on magnetic shielding.

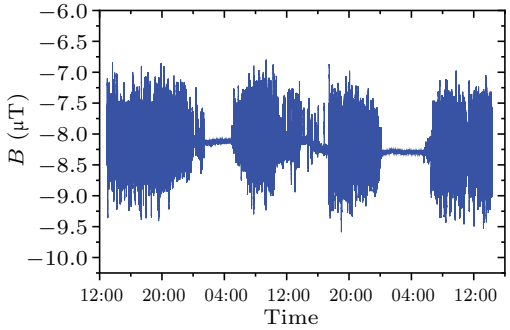


Fig. 3. Measurement of the magnetic field around the portable $^{40}Ca^+$ optical clock by Mag-03. It can be seen from the figure that the fluctuation of the magnetic field around the optical clock system reaches about 2.8 μT for most of the day, and only in a few hours at night, the fluctuation of the ambient magnetic field drops back to the level of about 0.1 μT. In other words, the magnetic field environment in which the optical clock operates has become about 30 times worse than the previous operating environment.

In order to more accurately evaluate the effect of active magnetic field noise suppression, we selected the $^2S_{1/2}(m_J = \pm 1/2)$– $^2D_{5/2}(m_J = \pm 5/2)$ transition, which is the most sensitive to the magnetic field among the three pairs of clock transition Zeeman components.[31,32] By scanning the associated parameter k, its optimal value was obtained by measuring the linewidth of the $^2S_{1/2}(m_J = \pm 1/2)$– $^2D_{5/2}(m_J = \pm 5/2)$ Zeeman transition. Then, the linewidths of the $^2S_{1/2}(m_J = \pm 1/2)$– $^2D_{5/2}(m_J = \pm 5/2)$ clock transition spectrum were measured under the conditions of the active magnetic field stabilization system turned on and off. Rabi spectroscopy was achieved with active magnetic field stabilization turned on, with a total clock interrogation time of 160 ms, which is much longer than a 5 ms clock interrogation time without active compensation. These results show that the active magnetic field noise compensation device further suppresses the magnetic field noise by more than 30 times, after the noise has been attenuated by more than 300 times by the magnetic shields.

Finally, by locking the frequency of the clock laser to the above Zeeman transitions with the Rabi excitation method, we also measured the frequency stability of the portable $^{40}Ca^+$ clock by the self-comparison method in the above two cases.

By linear fitting with a slope of -0.5, the stabilities are obtained as $2.3\times10^{-14}/\sqrt{\tau}$ and $2.5\times10^{-15}/\sqrt{\tau}$ (τ is the averaging time) when the active magnetic field stabilization system is turned off and on, respectively. Using the active compensation scheme for magnetic field noise, we have improved the frequency stability of previously limited transportable $^{40}Ca^{+}$ optical clocks[5,18] to the level of laboratory optical clocks.[20] This work is general and applicable not only to $^{40}Ca^{+}$ optical clocks, but to all magnetic field sensitive optical clocks. At the same time, it is more convenient to transport and less expensive than the full physical system magnetic shielding solution.[9] Further improvements in the portable clock stability require a portable probe laser with fractional frequency stability in the order of 10^{-16} at 1–200 s.[20]

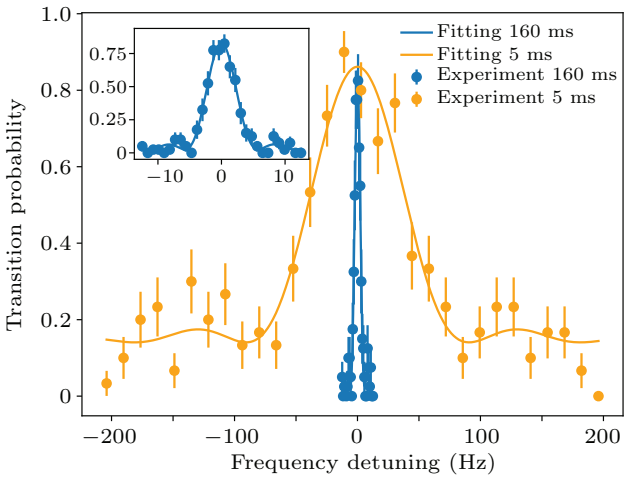


Fig. 4. Comparison of spectral lines when the active magnetic field suppression system is turned on and off. The blue and orange dots and lines represent the spectral lines when the magnetic field noise suppression system is turned on and off, respectively. The inner figure in the upper left corner is an enlargement of the spectral line when the magnetic field noise suppression system is turned on. Obviously, the contrast of the spectral lines corresponding to the 160 ms pulse length is better than that of the 5 ms pulse length.

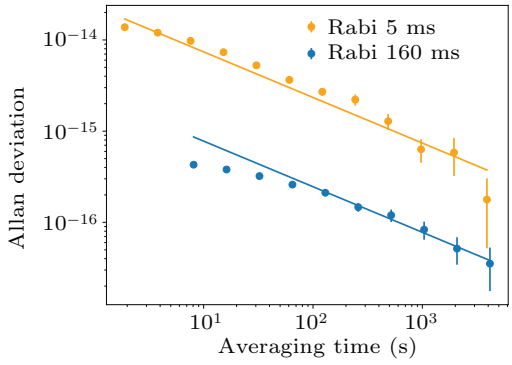


Fig. 5. Stability comparison between the active magnetic field stabilization system turned on and off. The orange and blue data points represent when the portable $^{40}Ca^{+}$ clocks are referenced to the transitions at $m_J=\pm5/2$. The orange solid line represents $2.3\times10^{-14}/\sqrt{\tau}$, while the overall clock interrogation time is 5 ms with the active magnetic field stabilization system turned off. The blue solid line represents $2.5\times10^{-15}/\sqrt{\tau}$, while the overall clock interrogation time is 160 ms with the active magnetic field stabilization system turned on.

5. Conclusion

Today, the uncertainty of the transportable $^{40}Ca^{+}$ optical clock has reached the 10^{-18} level, and the key to further improving its performance is to improve its stability outside the laboratory environment. To this end, we have developed passive and active magnetic field noise suppression systems. Based on multilayer magnetic shields, we have introduced a device that generates a reverse magnetic field by a current related to the external magnetic field noise, which further suppresses the magnetic field noise. Experimental measurements show that the improved passive magnetic shields can suppress the external magnetic field noise by more than 300 times. Together with the active magnetic field noise suppression device, it can further suppress the magnetic field noise by about 30 times. Then, the linewidth of the clock transition is narrowed to about 5 Hz, and the stability is improved to $2.5\times10^{-15}/\sqrt{\tau}$, which is equivalent to the stability obtained by the laboratory optical clock in a good magnetic environment.[20] In the future, the replacement of the magnetic field sensors with higher sensitivity is expected to further improve the noise suppression effect of the active feedback and achieve a longer optical clock interrogation time. This work improves the adaptability of transportable $^{40}Ca^{+}$ optical clocks to different magnetic field environments, significantly improves their stability, and lays a solid foundation for the wide application of transportable optical clocks.

Acknowledgements

This work is supported by the National Key R&D Program of China (Grant Nos. 2022YFB3904001, 2022YFB3904004, and 2018YFA0307500), the National Natural Science Foundation of China (Grant Nos. 12022414 and 12121004), the CAS Youth Innovation Promotion Association (Grant Nos. Y201963 and Y2022099), the Natural Science Foundation of Hubei Province (Grant No. 2022CFA013), the CAS Project for Young Scientists in Basic Research (Grant No. YSBR-055), and the Interdisciplinary Cultivation Project of the Innovation Academy for Precision Measurement of Science and Technology (Grant No. S21S2201).

References

[1] Brewer S M, Chen J S, Hankin A M, Clements E R, Chou C W, Wineland D J, Hume D B and Leibrandt D R 2019 *Phy. Rev. Lett.* **123** 033201

[2] Cui K F, Chao S J, Sun C L, Wang S M, Zhang P, Wei Y F, Yuan J B, Cao J, Shu H L and Huang X R 2022 *Eur. Phys. J. D* **76** 140

[3] Huntemann N, Sanner C, Lipphardt B, Tamm C and Peik E 2016 *Phys. Rev. Lett.* **116** 063001

[4] Huang Y, Zhang B L, Zeng M Y, Hao Y M, Ma Z X, Zhang H Q, Guan H, Chen Z, Wang M and Gao K L 2022 *Phy. Rev. Appl.* **17** 034041

[5] Zeng M Y, Huang Y, Zhang B L, Hao Y M, Ma Z X, Hu R M, Zhang H Q, Chen Z, Wang M, Guan H and Gao K L 2023 *Phys. Rev. Appl.* **19** 064004

[6] Zhang Z Q, Arnold K J, Kaewuam R and Barrett M D 2023 *Sci. Adv.* **9** 1971

[7] McGrew W F, Zhang X, Fasano R J, Schäffer S A, Beloy K, Nicolodi D, Brown R C, Hinkley N, Milani G, Schioppo M, Yoon T H and Ludlow A D 2018 *Nature* **564** 87

[8] Bothwell T, Kedar D, Oelker E, Robinson J M, Bromley S L, Tew W L, Ye J and Kennedy C J 2019 *Metrologia* **56** 065004

[9] Ohmae N, Takamoto M, Takahashi Y, Kokubun M, Araki K, Hinton A, Ushijima I, Muramatsu T, Furumiya T, Sakai Y, *et al*. 2021 *Adv. Quan. Technol.* **4** 2100015

[10] Lu B K, Sun Z, Yang T, Lin Y G, Wang Q, Li Y, Meng F, Lin B K, Li T C and Fang Z J 2022 *Chin. Phys. Lett.* **39** 080601

[11] Riehle F, Gill P, Arias F and Robertsson L 2018 *Metrologia* **55** 188

[12] Safronova M S, Budker D, DeMille D, Kimball D F J, Derevianko A and Clark C W 2018 *Rev. Mod. Phys.* **90** 025008

[13] Lange R, Huntemann N, Rahm J M, Sanner C, Shao H, Lipphardt B, Tamm C, Weyers S and Peik E 2021 *Phys. Rev. Lett.* **126** 011102

[14] Bothwell T, Kennedy C J, Aeppli A, Kedar D, Robinson J M, Oelker E, Staron A and Ye J 2022 *Nature* **602** 420

[15] Beloy K, Bodine M I, Bothwell T, Brewer S M, Bromley S L, Chen J, Deschênes J, Diddams S A, Fasano R J, Fortier T M, *et al*. 2021 *Nature* **591** 564

[16] Shen Q, Guan J, Ren J, Zeng L, Hou L, Li M, Cao Y, Han J, Lian M, Chen Y, *et al*. 2022 *Nature* **610** 661

[17] Grotti J, Koller S, Vogt S, Häfner S, Sterr U, Lisdat C, Denker H, Voigt C, Timmen L, Rolland A, *et al*. 2018 *Nat. Phys.* **14** 437

[18] Huang Y, Zhang H Q, Zhang B L, Hao Y M, Guan H, Zeng M Y, Chen Q F, Lin Y G, Wang Y Z, Cao S Y, Liang K, Fang F, Fang Z J, Li T C and Gao K L 2020 *Phys. Rev. A* **102** 050802

[19] Zhang B L, Huang Y, Zhang H Q, Hao Y M, Zeng M Y, Guan H and Gao K L 2020 *Chin. Phys. B* **29** 074209

[20] Zhang B L, Huang Y, Hao Y M, Zhang H Q, Zeng M Y, Guan H and Gao K L 2020 *J. Appl. Phys.* **128** 143105

[21] Dubé P, Madej A A, Zhou Z and Bernard J E 2013 *Phys. Rev. A* **87** 023806

[22] Takamoto M, Tanaka Y and Katori H 2022 *Appl. Phys. Lett.* **120** 140502

[23] Schkolnik V, Budker D, Fartmann O, Flambaum V, Hollberg L, Kalaydzhyan T, Kolkowitz S, Krutzik M, Ludlow A, Newbury N *et al*. 2023 *Quan. Sci. Technol.* **8** 014003

[24] Li L, Ji J W, Ren W, Zhao X, Peng X K, Xiang J F, Lü D S and Liu L 2016 *Chin. Phys. B* **25** 073201

[25] Farolfi A, Trypogeorgos D, Colzi G, Fava E, Lamporesi G and Ferrari G 2019 *Rev. Sci. Instrum.* **90** 115114

[26] Sumnert T J, Pendlebury J M and Smith K F 1987 *J. Phys. D Appl. Phys.* **20** 1095

[27] Jie S F, Li J L, Liu Z C and Mao Y K 2023 *Meas. Sci. Technol.* **34** 095124

[28] Merkel B, Thirumalai K, Tarlton J E, Schäfer V M, Balance C J, Harty T P and Lucas D M 2019 *Rev. Sci. Instrum.* **90** 044702

[29] Xiao K D, Wang L, Guo J, Zhu M H, Zhao X C, Sun X P, Ye C H and Zhou X 2020 *Rev. Sci. Instrum.* **91** 085107

[30] Duan Z X, Wu W T, Lin Y T and Yang S J 2022 *Rev. Sci. Instrum.* **93** 123201

[31] Tommaseo G, Pfeil T, Revalde G, Werth G, Indelicato P and Desclaux J P 2003 *Eur. Phys. J. D* **25** 113

[32] Barwood G P, Huang G, King S A, Klein H A and Gill P 2015 *J. Phys. B: At. Mol. Opt. Phys.* **48** 035401